Progress in Aerospace Sciences 68 (2014) 64–74

Contents lists available at ScienceDirect

Progress in Aerospace Sciences

journal homepage: www.elsevier.com/locate/paerosci

Survey of planetary entry guidance algorithms

Sarah N. D'Souza [1], Nesrin Sarigul-Klijn *

Space Engineering Research and Graduate Program (SpaceED), Mechanical and Aerospace Engineering Department, University of California Davis, 2132 Bainer Drive, Davis, CA 95616-5294, United States

ARTICLE INFO

Article history:
Received 15 October 2013
Received in revised form
26 January 2014
Accepted 30 January 2014
Available online 31 March 2014

Keywords:
Entry guidance
Hypersonic
Guidance
Navigation control
Entry spacecraft

ABSTRACT

This comprehensive literature survey reviews past and present planetary entry guidance algorithms. The algorithms are categorized based on the vehicle L/D and the planetary atmosphere that the vehicle is entering. Each algorithm is described based on the guidance type, the guidance formulation, and the inclusion of aerothermal parameters. An analysis was completed defining the performance of each guidance algorithm relative to one another within its specific category. Finally, an overall assessment was made regarding the state-of-the-art in spacecraft entry guidance.

Contents

1. Introduction

The entry guidance algorithm for lunar return of the manned Apollo capsule (1960s) was the first flight tested application of guidance. Since the pioneering efforts of Apollo guidance engineers, many algorithms have been developed for different missions and vehicles. However, there are no publications that comprehensively discuss the types of guidance algorithms and their formulations. This paper details past and present guidance algorithms in three categories: (1) high L/D, Earth entry spacecraft, (2) low- to mid-L/D, Earth entry spacecraft, and (3) other planetary entry spacecraft. In each category, the vehicle and entry trajectory type are defined, see Fig. 1 for an illustration of different vehicle types. Entry trajectories include aerocapture, direct entry, lofted entry, and skip entry. It should be noted that the objective of an

* Corresponding author. Tel.: +1 530 752 0682.
E-mail address: nsarigulklijn@ucdavis.edu (N. Sarigul-Klijn).
[1] Preesntly Aerospace Flight Systems Engineer. NASA Ames Research Center.

http://dx.doi.org/10.1016/j.paerosci.2014.01.002
0376-0421

Nomenclature

D	drag acceleration (ft/s^2)
D_f	drag force (lbf)
$\vec{F}$	force vector (lbf)
F_t	total force orthogonal to velocity vector (lbf)
F_t	total force parallel to velocity vector (lbf)
g	gravitational acceleration [ft/s^2]
h	altitude (ft)
L	lift acceleration [ft/s^2]
L_f	lift force (lbf)
m	vehicle mass (lbm)
R	magnitude of the radial distance vector for 3RSP model (ft)
$\vec{R}$	radial distance vector (ft)
t	time (s)
T_p	propulsive force (lbf)
V	relative velocity (ft/s)
x	downrange (nmi)
y	crossrange (nmi)
ϵ	angle between $\vec{v}_r$ and $\vec{F}$ (deg)
ϕ	declination (deg)
γ	flight path angle (deg)
θ	longitude (deg)
σ	bank angle (deg)
$\vec{\Omega}$	planet's rotation vector (1/rad)
ψ	azimuth (deg)
ACRV	assured crew return vehicle
AOTV	aeroassist orbit transfer vehicle
CAV	common aero vehicle
COV	calculus of variations
HEMS	high entry mass systems
MaRV	maneuvering re-entry vehicle
MER	Mars exploration Rover-class
MOrb	Mars 2001 orbiter
MSP	Mars surveyor program
SC	sphere cone

aerocapture trajectory is to meet a desired orbit, while a direct/lofted/skip trajectory is performed to target a specific landing site on the planet surface, but both require a guidance algorithm to be meet these targets.

Typically, guidance algorithms developed for Low L/D (<0.5) vehicles fly short range trajectories with moderate payloads ($\sim$5000 kg). Guidance algorithms, developed for high L/D (≥ 1.0) spacecraft can fly a longer cross range, perform a runway landing, and carry very large payloads to the ground (upwards of 10,000 kg). Guidance algorithms for Mid-L/D (≥ 0.5 and <1.0) vehicles have been of recent interest because larger payloads can be guided to the ground while maintaining low heat rates and low deceleration at higher altitudes. Although the reachable range for entry is dependent on guidance, it is more of a direct function of the spacecraft capability and the entry trajectory type. Some well known examples of low L/D spacecraft are Apollo, Mars Science Laboratory (MSL), and SpaceX's Dragon Capsule. The only high L/D spacecraft that has been extensively flight tested and used is NASA's now retired Space Shuttle, whereas most others are experimental. Mid L/D spacecraft are currently being examined for future high mass missions to Mars. There are other advancements in the works with the increase in the commercialization of space and developments in military hypersonics projects. However, many of these advanced guidance algorithms have yet to be published in publicly available journals.

This paper begins with an introduction to the field of entry guidance and then discusses the various models used to model entry flight dynamics. Finally, a comprehensive discussion of the state-of-the art in entry guidance is documented and discussed.

2. Fundamentals of entry guidance development

The construct for analysis of past and present guidance algorithms is derived from the process of guidance algorithm development. Guidance development can be a relatively subjective process as there are numerous ways to use the equations of motions and numerous requirements for a given mission.

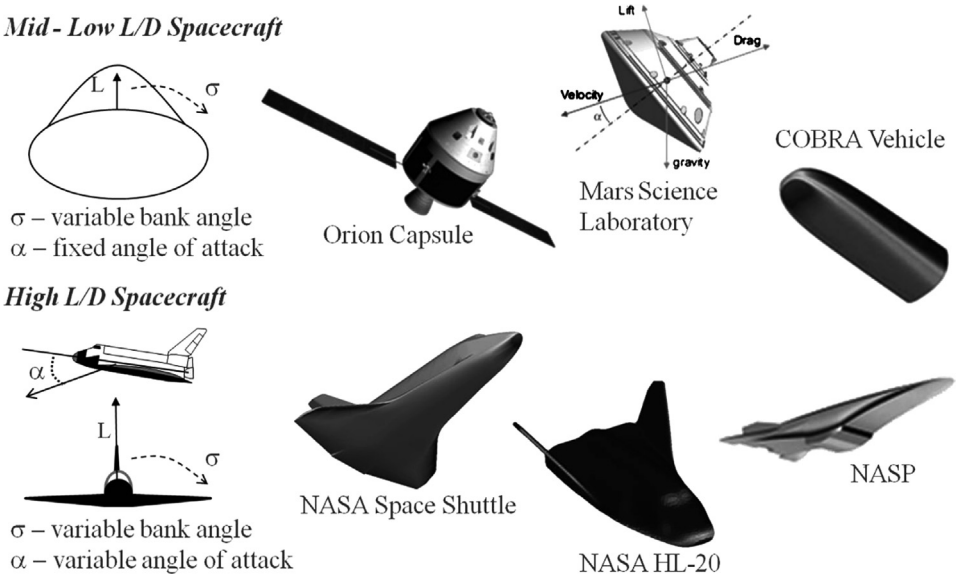

Fig. 1. Shape and available controls for different vehicle shapes.

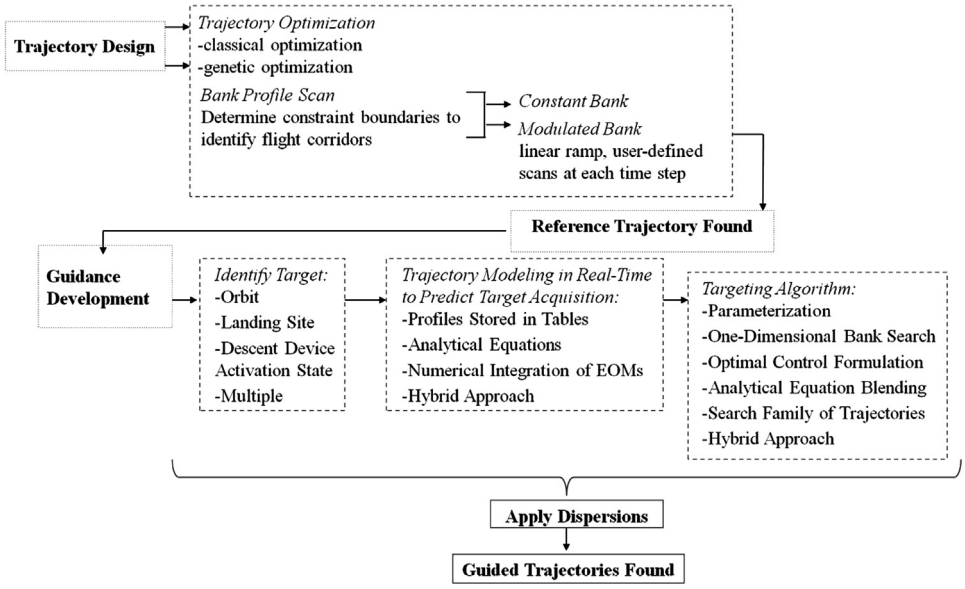

Fig. 2. Trajectory design and guidance development chart.

Table 1
The dis/advantages of analytical and numerical formulations.

Analytical formulation	Numerical formulation
Advantages	
Simple to implement	Accurate trajectory solutions
Computation time minimal	No simplifying assumptions
Solution guaranteed	
Disadvantages	
Low fidelity trajectory solution	Convergence is not assured
Formulation tied to a specific entry case	Extended convergence times

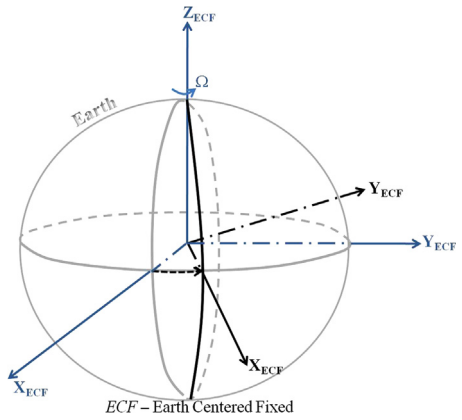

Fig. 3. Earth Centered Fixed coordinate system.

The flow chart in Fig. 2 describes the process of re-entry guidance development.

The first step to developing a guidance algorithm is to design a trajectory that takes the vehicle from the entry interface to the target state within pre-defined constraints and mission requirements. This trajectory design is the baseline that allows for accurate validation of the nominal guidance algorithm. Guidance algorithms must also meet the following in-flight requirements during the process of development:

1. Determine flight feasible control vectors (control rate/acceleration constraints).
2. Be highly robust to dispersions and perturbations.
3. Predict trajectory with high precision and quickly.
4. Acquire target with high precision and quickly.

The last two criteria highlight two key components in guidance development: trajectory prediction and targeting. Trajectory prediction requires the developer to define the trajectory path with just enough detail to precisely identify whether the vehicle will meet its target. The accuracy of this prediction is dependent on the fidelity of the formulation relative to the entry vehicle, desired trajectory, and available navigational inputs. Note that during the Apollo era, the guidance formulation could not necessarily use high fidelity EOMs due to the limited computing power of the 1950s and 1960s. Thus, the Apollo guidance formulation was a compact set of closed-form analytical equations that tracked to a reference trajectory which was stored as a table. As computing power became exponentially larger, guidance formulations evolved into numerical solutions integrated with analytical equations, optimization methods, search routines, and neural networks. For example, the requirements that NASA's Orion spacecraft complete a lunar return in the contiguous United States and have an increased payload from Apollo [1], necessitated the development of numerical guidance algorithms. These algorithms had to achieve extended range, which the Apollo Guidance was not robust enough to achieve. Despite these changes, there are advantages and disadvantages to purely analytical and purely numerical formulations, which are summarized in Table 1.

The primary disadvantage to analytical guidance algorithms is the application of several simplifying assumptions. The assumptions make the guidance algorithm less robust to a wider range of dispersions. In addition, the ability to increase the entry range or change the vehicle aerodynamics is restricted because the assumptions make the formulation invalid for those changes. The primary advantage of analytical guidance is its simplicity and fast solution time. Given the fast timeline for hypersonic entry, these features are desirable. Primary disadvantages of numerical formulations include the possibility of no convergence to a solution or extended convergence times to a solution. This is not acceptable since the hypersonic entry of a spacecraft is rapid and a control solution must be determined quickly for a precision landing.

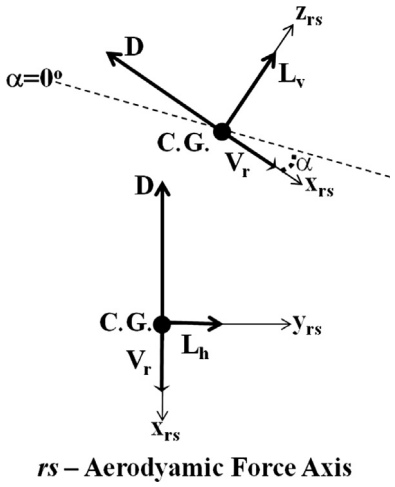

Fig. 4. Aerodynamic force axis system.

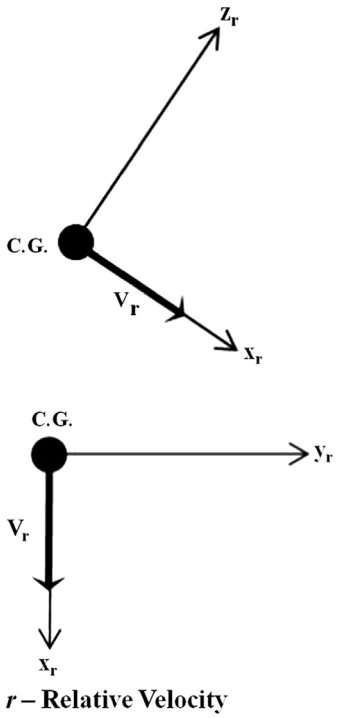

Fig. 5. Relative Velocity Coordinate system.

The objective of the second key guidance component, targeting, is to calculate the control necessary to bring the vehicle into a path that meets the target, without violating loading constraints and control system constraints. The targeting methodology is also subjective to the developer's viewpoint of what will be the quickest, most efficient method to find a new trajectory solution in real-time. The flow chart in Fig. 2 identifies trajectory prediction and targeting separately for general understanding of guidance development. However, prediction and targeting are not mutually exclusive and the interaction of these components with one another is dependent on the developers proposed guidance method.

2.1. Entry flight dynamics and the equations of motion

The guidance algorithms surveyed in this paper were, in part, analyzed by the set of equations used to model the predicted trajectory. The accuracy of the trajectory prediction and targeting algorithms depends on the fidelity of the models and the equations of motion (EOMs) it uses. The following sections discuss EOMs of varied fidelity.

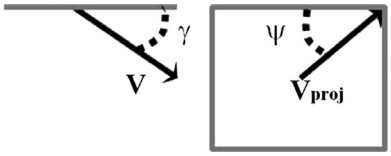

Fig. 6. Relative velocity with respect to horizontal plane.

2.1.1. 3DOF rotating, spherical planet (3RSP) EOMs

The derivation of this set of equations can be found in Vinh [2]. Note that the planet is assumed to be spherical and the coordinate systems in the two body problem correspond to relative motion dynamics. The Earth coordinate frame is fixed at the origin and rotates with the Earth (Fig. 3), where the X_{ECF}-axis is located in the plane of the Equator and is pointed toward the longitude at the start of the trajectory. The Y_{ECF}-axis is perpendicular to the X_{ECF}-axis and the Z_{ECF}-axis completes the right handed set. There are two vehicle axes whose origin is at the vehicle's center of gravity. First, there is the axis system that is defined with respect to the aerodynamic forces. The y-axis is parallel to the velocity vector, the x-axis is parallel to the vertical lift component, and the z-axis is parallel to the horizontal lift component (Fig. 4).

Second, the relative velocity (r) reference system describes the motion of the vehicle with respect to the free stream. The positive x-direction is parallel to the relative velocity vector, the positive y-direction points toward the right (perpendicular to the position vector), and the z-direction completes the right-handed system (Fig. 5). If it is assumed that there are no side forces then the x_{rs}-axis coincides with the x_r-axis and the bank angle is a rotation purely about the x_{rs}-axis.

The derivation of the EOMs can now be carried out, beginning with the position vector (1) illustrated in Fig. 7:

$$\vec{R} = R\hat{i}_r \tag{1}$$

The vector $\vec{R}$ is parallel to the x_r-axis. The time derivative is applied to Eq. (1), which results in the following equation:

$$\frac{{}^{i}d\vec{R}}{dt} = \vec{v}_r = \frac{{}^{r}d\vec{R}}{dt} + \vec{\Omega} \times \vec{R} \tag{2}$$

Note that the derivative was taken with respect to the coordinate frame indicated in the superscript to the left of the derivatives. The relative velocity vector (3) is a function of the speed of the vehicle, its flight path angle relative to the horizontal plane (Fig. 6), and the heading angle within the horizontal plane:

$$\vec{v}_r = V \sin\gamma\hat{i}_r + V\cos\gamma\sin\psi\hat{j}_r + V\cos\gamma\cos\psi\hat{k}_r \tag{3}$$

Next, the time derivative of the velocity vector is taken to get the relative acceleration vector:

$$\frac{{}^{i}d\vec{v}_r}{dt} = \frac{{}^{r}d^2\vec{R}}{dt^2} + 2\vec{\Omega} \times \frac{{}^{r}d\vec{R}}{dt} + \vec{\Omega} \times (\vec{\Omega} \times \vec{R}) \tag{4}$$

The acceleration equation (4) includes several terms on the right hand side, the first term is the acceleration of the vehicle, the second term is the Coriolis acceleration, and the third term is the centripetal acceleration, all in the relative coordinate system. Next, Eq. (4) is multiplied by the mass of the vehicle resulting in the total force equation:

$$\vec{F} = m\frac{{}^{r}d^2\vec{R}}{dt^2} + 2m\vec{\Omega} \times \frac{{}^{r}d\vec{R}}{dt} + m\vec{\Omega} \times (\vec{\Omega} \times \vec{R}) \tag{5}$$

Note that the Earth's rotation vector in the relative coordinate system is as follows:

$$\vec{\Omega} = \Omega \sin\phi \hat{i}_r + \Omega \cos\phi \hat{k}_r \tag{6}$$

The force vector $(\vec{F})$ consists of gravitational, aerodynamic, and propulsive forces. The gravity force is acting along the x-axis in the relative coordinate system and gravitational acceleration $(\vec{g})$ is calculated assuming a spherical Earth. The aerodynamic and propulsive forces are acting along and orthogonal to the velocity vector. The magnitude of the force acting along the velocity vector is

$$F_t = T_p \cos\epsilon - D_f \tag{7}$$

The magnitude of the force acting orthogonal to the velocity vector is

$$F_n = T_p \sin\epsilon + L_f \tag{8}$$

Since F_t is also acting in the direction of the velocity vector, Eq. (3) can be used to write $\vec{F}_t$ in relative coordinates:

$$\vec{F}_t = F_t \sin\gamma \hat{i}_{rs} + F_t \cos\gamma \sin\psi \hat{j}_{rs} + F_t \cos\gamma \cos\psi \hat{k}_{rs} \tag{9}$$

The force orthogonal to the velocity vector is expressed in relative coordinates by applying transformation matrices to $\vec{F}_n$ in the rs-coordinate system (10):

$$\vec{F}_n = F_n \cos\sigma \hat{i}_r + F_n \sin\sigma \hat{k}_r \tag{10}$$

The bank angle is a rotation about the velocity vector, which is measured between the lift vector and the x_{rs}-axis. The transformation matrices correspond to a rotation ψ in the horizontal plane followed by a rotation γ in the vertical plane. The results are as follows:

$$\vec{F}_N = F_N \cos\sigma \cos\gamma \hat{i}_{rs} - (F_N \cos\sigma \sin\gamma \cos\psi + F_N \sin\sigma \sin\psi)\hat{j}_{rs} - (F_N \cos\sigma \sin\gamma \sin\psi - F_N \sin\sigma \cos\psi)\hat{k}_{rs} \tag{11}$$

After considerable manipulation of Eqs. (2)–(11), a set of six ordinary differential equations are derived:

$$\dot{R} = V \sin\gamma \tag{12}$$

$$\dot{\theta} = \frac{V \cos\gamma \sin\psi}{R \cos\phi} \tag{13}$$

$$\dot{\phi} = \frac{V \cos\gamma \cos\psi}{R} \tag{14}$$

$$\dot{V} = -D - g \sin\gamma + \Omega^2 R \cos\phi(\sin\gamma \cos\phi - \cos\gamma \sin\phi \cos\psi) \tag{15}$$

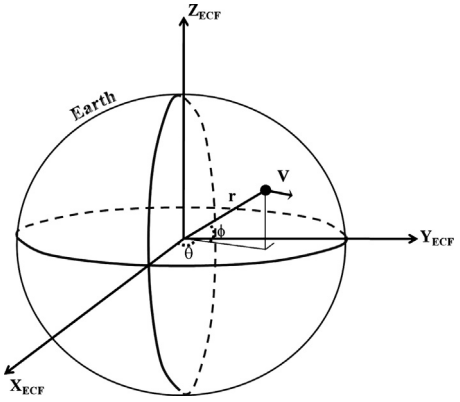

Fig. 7. Position vector with respect to the Earth's center.

$$\dot{\gamma} = \frac{1}{V}\left[L \cos\sigma + \cos\gamma\left(\frac{V^2}{R} - g\right) + 2\Omega V \cos\phi \sin\psi + \Omega^2 R \cos\phi(\cos\gamma \cos\phi + \sin\gamma \cos\psi \sin\phi)\right] \tag{16}$$

$$\dot{\psi} = \frac{1}{V}\left[\frac{L \sin\sigma}{\cos\gamma} + \frac{V^2}{R} \cos\gamma \sin\psi \tan\phi - 2\Omega V(\tan\gamma \cos\psi \cos\phi - \sin\phi) + \frac{R\Omega^2}{\cos\gamma} \sin\psi \sin\phi \cos\phi\right] \tag{17}$$

Eqs. (12)–(17) are considered high fidelity.

2.1.2. 3DOF non-rotating, spherical earth (3NSP) EOMs

This set of equations follows from assuming that the Earth's rotation is negligible. Thus the EOMs are as follows:

$$\dot{R} = V \sin\gamma \tag{18}$$

$$\dot{\theta} = \frac{V \cos\gamma \sin\psi}{R \cos\phi} \tag{19}$$

$$\dot{\phi} = \frac{V \cos\gamma \cos\psi}{R} \tag{20}$$

$$\dot{V} = -D - g \sin\gamma \tag{21}$$

$$\dot{\gamma} = \frac{1}{V}\left[L \cos\sigma + \cos\gamma\left(\frac{V^2}{R} - g\right)\right] \tag{22}$$

$$\dot{\psi} = \frac{1}{V}\left[\frac{L \sin\sigma}{\cos\gamma} + \frac{V^2}{R} \cos\gamma \sin\psi \tan\phi\right] \tag{23}$$

Note that all the terms containing Earth's rotation have been ignored.

2.1.3. 3DOF non-rotating, flat earth (3NFP) EOMs

This set of equations makes the assumption that the Earth is flat in addition to the non-rotating Earth assumption. In Vinh [3], the flat Earth assumption is applied such that a slice of the planet is taken at the Equator, $\phi = 0$. Thus, the EOMs now take the form:

$$\dot{h} = V \sin\gamma \tag{24}$$

$$\dot{x} = V \cos\gamma \cos\psi \tag{25}$$

$$\dot{y} = V \cos\gamma \sin\psi \tag{26}$$

$$\dot{V} = -D - g \sin\gamma \tag{27}$$

$$\dot{\gamma} = \frac{1}{V}\left[L \cos\sigma + \cos\gamma\left(\frac{V^2}{R} - g\right)\right] \tag{28}$$

$$\dot{\psi} = \frac{L \sin\sigma}{V \cos\gamma} \tag{29}$$

2.1.4. 2DOF Longitudinal (2LON) EOMs

The most obvious difference between this set of EOMs and the above is the reduced dimensionality. The lateral (crossrange) and longitudinal (downrange) motion are decoupled in order to simplify the problem. The assumption of a non-rotating, flat Earth holds for this set of EOMs

$$\dot{h} = V \sin\gamma \tag{30}$$

$$\dot{s} = V \cos\gamma \tag{31}$$

$$\dot{V} = -D - g \sin \gamma \tag{32}$$

$$\dot{\gamma} = \frac{1}{V}\left[L \cos \sigma + \cos \gamma \left(\frac{V^2}{R} - g\right)\right] \tag{33}$$

Table 2
Equations of motion for planetary entry ordered from higher to lower fidelity.

3RSP	3DOF Rotating, spherical planet	High fidelity
3NSP	3DOF Non-rotating, spherical planet	
3NFP	3DOF Non-rotating, flat planet	
2LON	2DOF Longitudinal	Low fidelity

Neglecting lateral motion eliminated the azimuth rate equation and results in a differential equation for the total range (s [nmi]). Eqs. (30)–(33) define only the longitudinal motion of the vehicle.

3. Entry guidance survey categories and definitions

An understanding of the fundamentals of entry guidance provides a window by which to analyze the heritage and modern guidance algorithms surveyed in this paper. Each guidance algorithm was reviewed with respect to three characteristics:

1. *Guidance type* – guidance algorithms can be of many different types, namely:

Table 3
High L/D entry spacecraft guidance algorithms.

Test case: (Vehicle) mission	Guidance type	Guidance formulation	Aerothermal inclusion
(**X-33**, $L/D \geq 1.0$)[a] Refs. [4–6] *Direct entry*	In-flight reference generation and tracking	Numerically solve the 3RSP EOMs to determine feasible reference trajectories using drag/bank reversal planning (two parameter search and mapping techniques). Track reference using 2nd order tracking law for linear error	Heat rate is a vehicle constraint accounted for during trajectory planning
(**X-33**, $L/D \geq 1.0$)[a] Refs. [7,9,10] *Direct entry*	In-flight controls search/reference tracking	Numerically solve the 3RSP EOMs by incorporating a trajectory-segmenting scheme in tandem with an equilibrium glide condition (2LON) and secant search method to determine the control vector. A closed-form approximate receding-horizon control law based on linearized time-varying dynamics. The EOMs used to derived the control law: Ref [9] – 3RSP; Ref. [10] – 3NSP	Heat rate is a constraint included in the reference trajectory generation
(**X-33**, $L/D \geq 1.0$)[b] Refs. [11] *Direct entry*	In-flight reference generation and tracking	Generates reference trajectory by solving the 2-point boundary value reentry problem with a multi-dimensional root finding algorithm and the 3RSP EOMs	The first phase of entry incorporates a heat rate tracking law for a constant reference heat rate
Direct entry (**X-33**, $L/D \geq 1.0$)[b] Refs. [12] *Direct entry*	Reference tracking	Linear quadratic regulator using 2LON EOMs	Heat rate is a constraint considered in off-line trajectory optimization
(**X-33**, $L/D \geq 1.0$)[c] Ref. [13] *Direct entry*	Reference tracking	2LON EOMs applied to range control using drag based approximations w/ damped harmonic oscillator control law	Heat rate constraint in trajectory design
(**X-33**, $L/D \geq 1.0$) Ref. [14,15] (**X-34**, $L/D \geq 1.0$) Ref. [27] (**X-40A**, $L/D \geq 1.0$)[d] Ref. [21] *Direct entry*	In-flight trajectory shaping/ reference tracking	Interrogation of stored PNN database w/ optimization to shape the reference trajectory. Uses COV on 2LON EOMs	None specifically stated
(**X-33**, $L/D \geq 1.0$)[e] Ref. [8] *Direct entry*	Analytical optimization/ reference tracking	Analytical drag approximations w/ optimization, no specific EOMs needed for integration	Heat rate constraint used in optimization and heat load is combined with range in the objective function during optimization
(**NASA Space Shuttle**, $L/D \geq 1.0$)[d] Refs. [17,18] *Direct entry*	Reference tracking	Analytical closed form solutions for the 2LON EOMs that are specific to each phase of the entry profile	Drag quadratic coefficients, for the temperature phase, are derived from heat rate limits
(**NASA Space Shuttle**, $L/D \geq 1.0$)[e] Ref. [26] *Direct entry*	In-flight reference planning and tracking	Generate reference trajectories by solving an optimization problem using 3NSP EOMs with drag and lateral acceleration as intermediate controls	Heat rate and heat load are used as soft constraints during optimal trajectory planning
(**IXV**, $L/D \geq 1.0$) Ref. [28] *Skip/direct entry*	Reference tracking	Numerically solve the 3RSP EOMs where bank modulation is a function of energy and range	Max. Heat Rate and max. Heat load are defined as mission requirements
(Launch) Ref. [22,23] (**MaRV**, $L/D \geq 1.0$) Ref. [24] (**CAV**, $L/D \geq 1.0$) Ref. [25] *Direct entry*	In-flight optimization (Unsimplified)	The Legendre Pseudospectral Method is a hybrid of indirect and direct numerical methods, which converts the optimal control problem to an NLP problem for fast convergence. The EOMs, constraints, and objectives are identified by the user for the given problem	None specifically stated, Ref. [22–24]. Heat rate is included as a constraint during optimization [25]
(**HORUS**, $L/D \geq 1.0$) Ref. [29] *Direct entry*	Reference tracking	Reference trajectory consists of energy as a function of the distance-to-target and several control parameters/gains. The energy and altitude control laws are based on classical controls	Heat rate and heat load are constraints used during off-line optimization of the reference trajectory and control parameters

[a] High robustness.
[b] Moderate robustness.
[c] Low robustness.
[d] Flight tested.
[e] Managed heat load.

Table 4
Mid- to low-L/D entry spacecraft guidance algorithms.

Test case: (vehicle) mission	Guidance type	Guidance formulation	Aerothermal inclusion
(**CEV**, $L/D<1.0$)[a] Refs. [31,32,34,42] *Skip/loft/direct entry*	In-flight controls search/reference tracking	Skip – Numeric predictor–corrector which integrates the 3RSP EOMs and iterates on bank to null range error. Direct – COV using 2LON EOMs w/ reference trajectory database	Heat rate and heat load are monitored parameters
(**CEV**, $L/D<1.0$)[b] Refs. [30,35] *Skip/direct entry*	In-flight controls search/reference tracking	Skip – numerically solve the 3RSP EOMs w/ one dimensional bank search. Direct – COV using 2LON EOMs w/ reference trajectory database	Heat Rate is a monitored parameter
(**Apollo**, $L/D<1.0$)[c] Refs. [38,39] *Direct entry* (**CEV**, $L/D<1.0$)[d] Refs. [36] *Skip/loft/direct entry*	Reference tracking	COV using 2LON EOMs w/ closed form analytical solutions and reference trajectory database (adapted from Apollo Guidance)	None specifically stated
(**CEV**, $L/D<1.0$) Ref. [33] *Skip/loft/direct entry*	In-flight controls search	Skip – numerical solution to 3RSP EOMs, bank modulation is linear and the initial bank search is a nonlinear univariate root-finding problem Direct – numerically solve 2LON EOMs w/ one dimensional bank search using Newton–Raphson	None specifically stated
(**CEV**, $L/D<1.0$) Ref. [37] *Skip/loft/direct entry*	In-flight controls search	Numerically solve 2LON EOMs w/ one dimensional bank search using Newton–Raphson	Author states that no heat rate constraint is needed since maximum g-load occurs first
(**CEV**, $L/D<1.0$) Ref. [37] *Skip/loft/direct entry*	In-flight controls search	Numerically solve 3RSP EOMs w/ two dimensional search using Newton–Raphson	Author states that no heat rate constraint is needed since maximum g-load occurs first
(**ARD**, $L/D<1.0$) Ref. [28] *Skip/direct entry*	Reference tracking	Numerically solve the 3RSP EOMs where bank modulation is a function of energy and range	Max. Heat Rate and max. Heat Load are defined as mission requirements
(**ACRV**, $L/D<1.0$) Ref. [43]	Reference tracking	Linear quadratic regulator using 2LON EOMs	Heat rate is a constraint considered in off-line trajectory optimization

[a] High robustness.
[b] Moderate robustness.
[c] Flight tested.
[d] Low robustness.

Stored reference tracking – stored reference trajectory variables and determine controller gains for tracking.
In-flight reference generation and tracking – represent reference trajectory analytically or store in tables, then modify in-flight to acquire target.
In-flight controls search – predict the trajectory numerically and perform one-dimensional search to acquire target.
In-flight optimal control – apply optimization techniques such that an optimal control solution is found to null targeting errors.

2. *Guidance formulation* – the formulation can be analytical and/or numerical to determine the vehicle flight path, range to target, and control solution. These variables are found using any of the equations of motion (EOMs) given in Table 2.
3. *Aerothermal inclusion* – indicates whether the guidance algorithm includes monitoring and/or management of heat rate and/or heat load.

The guidance algorithms surveyed are detailed in Tables 3–5. Note the following features of these tables:

- References with specific symbols indicate robustness: '†'=high robustness, '‡'=moderate robustness, and '§'=low robustness. The order of robustness is based on the available comparative studies to-date.
- References without symbols may still be very robust, but have not been directly compared to other algorithms.
- References that include the symbol '*' indicate guidance algorithms that have included techniques to manage heat load.
- Algorithms that have double asterisks (**) indicate that this algorithm has been flight-tested (on-board and/or in-flight simulators).

Note that the authors of this publication welcome any feedback relating to the technical content of this survey.

4. Entry guidance survey results

4.1. High L/D earth entry vehicles

There are several different high L/D vehicles for which guidance algorithms have been developed. In particular, several guidance algorithms [4–15] have been developed for the X-33, a sub-orbital reusable launch vehicle performing a direct entry. A comparative robustness study [16] of these algorithms was completed and it was found that the most robust algorithms are used in-flight reference generation and tracking techniques. These guidance algorithms used a combination of numerical and analytical formulations derived from the 3RSP EOMs (Eqs. (12)–(17)). Whereas the least robust algorithms contained analytical formulations derived from the 2LON EOMs (Eq. (30)–(33)) and used reference tracking only. The use of the 2LON EOMs assumes decoupled longitudinal and lateral motion. It is interesting to note that the baseline guidance algorithm for this comparative study was derived from the Shuttle Entry Guidance (SEG) algorithm [17,18] and was found to be the least robust. The SEG algorithm uses a reference tracking technique that adjusts the reference trajectory in-flight and is a purely analytical formulation derived from the 2LON EOMs. Despite the reduced robustness of the SEG many guidance developers take advantage of the drag acceleration approach, including but not limited to Refs. [4,5,19,20]. This approach describes the reference trajectory in terms of the drag acceleration profile, which is developed from a known nominal trajectory.

Table 5
Other planetary entry spacecraft guidance algorithms.

Test case: (vehicle) mission	Guidance type	Guidance formulation	Aerothermal inclusion
(**MSLab**, $L/D<1.0$)[a] Ref. [52] *Direct entry, Mars* (**TBB**, $L/D<1.0$)[b] Ref. [54] *Aerocapture, Titan* (**MSLan**, $L/D<1.0$)[a] Ref. [51] *Direct entry, Mars* (**MPrm**, $L/D<1.0$)[b] Ref. [50] *Aerocapture, Mars* (**MOrb**, $L/D<1.0$)[b] Ref. [44] *Aerocapture, Mars*	Reference tracking	COV using 2LON EOMs w/ reference trajectory database (adapted from Apollo Guidance)	Heat rate constraint in trajectory design
(**HEMS**, $L/D<1.0$) Ref. [55] *Aerocapture, Mars* (**NEV**, $L/D<1.0$) Ref. [53] *Aerocapture, Neptune* (**TBB**, $L/D<1.0$)[b] Ref. [54] *Aerocapture, Titan* (**MPrm**, $L/D<1.0$)[b] Ref. [50] *Aerocapture, Mars* (**MSR**, $L/D<1.0$) Ref. [46] *Aerocapture, Mars* (**MSR**, $L/D<1.0$) Ref. [45] *Direct entry, Mars* (**AOTV**, $L/D\geq 1.0$) Ref. [41] *Aeroassist, Mars*	Reference tracking	Analytical predictor–corrector using closed form solutions to the 2LON EOMs, w/ reference trajectory calculated in-flight	None specifically stated, Refs. [41,45,46,54,50,55]. Heat rate and heat load are monitored parameters, Ref. [53]
(**MSR**, $L/D<1.0$)[b] Refs. [47] *Aerocapture, Mars*	Reference tracking	This algorithm relates the 2DOF EOMs to Keplerian motion EOMs [61, Chapter 1] to generate a closed form solution that commands a specific bank angle	None specifically stated
(**MSP**, $L/D<1.0$)[c] Refs. [48,62] *Aerocapture/direct entry, Mars* (**MSR**, $L/D<1.0$)[c] Refs. [49] *Aerocapture, Mars*	In-flight controls search	Numerically solve the 3RSP EOMs using a command vector that includes roll angle magnitudes and reversal times	None specifically stated
(**MSLab**, $L/D<1.0$) Ref. [63] *Direct entry, Mars*	Reference tracking	Linearization of the 3NSP EOMs used to develop a state-dependent Riccati equation tracking controller	None specifically stated
(**MSLab**, $L/D<1.0$ MSP, $L/D\leq 1.0$) Refs. [56,57] *Direct entry, Mars*	Reference tracking	Range prediction and control law derived from 2LON EOMs w/ polynomial drag approximation as a function of energy	None specifically stated
(**SC**, $L/D=N/A$) Refs. [58] *Aerocapture, Mars* (**MER**, $L/D=N/A$) Refs. [59] *Direct entry, Mars*	In-flight controls search, drag modulation	Trajectory prediction numerically solves the 3RSP EOMs using fourth order Runge–Kutta, except the planet is assumed to be an oblate spheroid. Targeting then iterates on the control(s), jettison time (and change in ballistic coefficient), until the range error is within the tolerance. Note that this technique is applied to an Earth Aerocapture in [58]	None specifically stated
(**Biconic**, $L/D<1.0$)[d] Ref. [60] *Aerocapture, Neptune*	In-flight control optimization	Numerically solve 3RSP EOMs, where [σ α] pairs for specific phases are optimized to null the range error	Heat load constraint is one of four variables used to trigger targeting routine
(**MSLab**, $L/D<1.0$) Ref. [64] *Direct entry, Mars*	Reference tracking	The reference trajectory is represented as a fourth order polynomial approximation of altitude as a function of range-to-go. From this profile, a reference flight path angle and energy profile is derived using the 2LON EOMs	None specifically stated

[a] Flight tested.
[b] High robustness.
[c] Low robustness.
[d] Managed heat load.

Scheirman et al. [21] applied their X-33 adaptive guidance to Boeing X-40A and was tested on the general dynamics total in-flight simulator. This method uses in-flight trajectory shaping and reference tracking techniques to not only account for dispersions but for control failures as well. A database of trajectories in the form of Polynomial Neural Networks (PNN) is compiled off-line. Then the reference trajectory is re-shaped in-flight by interrogating the PNN and performing an optimization to converge to a feasible solution. This formulation uses a combination of analytical and numerical techniques.

An in-flight optimization method has been developed using Pseudospectral Methods [22–25]. This is a predominantly numerical method and has been theoretically applied to launch vehicles and re-entry problems due in part to its fast convergence. However, it is still unclear whether the fast convergence is fast enough for a planetary entry problem.

Typically, developing guidance for high L/D spacecraft requires the engineer to include some constraint or control on the peak heat rate. This is apparent in almost all of the guidance algorithms noted in Table 3. Guidance developers are rarely concerned with managing heat load, which makes sense given that precision landing is of primary concern. However, there are two algorithms which actually manage the heat load within the guidance algorithm. The first is Lu and Hanson [8] an analytical guidance algorithm which formulates an optimal control problem that minimizes range error and heat load. The second is Mease et al. [26] which includes a soft constraint on heat load in the guidance trajectory planner.

4.2. Mid- to low-L/D earth entry vehicles

There have been many papers published on guidance algorithms developed for the Crew Exploration Vehicle (CEV), including [30–34]. There are two different studies, Refs. [35,36], that compare the performance of numerical and analytical guidance algorithms performing a skip trajectory. There is also a study [37] that compares the performance of guidance algorithms that use EOMs of different fidelity for CEV performing a direct entry. In Ref. [36] it was found that the adapted Apollo Skip Entry Guidance, which is purely analytical, is the least robust relative to the numeric predictor–corrector guidance. The numeric predictor–corrector solves the 3RSP EOMS and performs a one parameter search to meet critical points in the trajectory. It should be noted that this is only for entry trajectories that require a skip maneuver. In Ref. [35] the performance of two guidance algorithms for CEV was compared. The primary difference between these algorithms was the event transition logic, but both use a numeric predictor–corrector coupled with the Apollo Final Phase

logic. It was found that the more robust guidance algorithm used the Apollo event transition logic during a skip entry. In Ref. [37] the performance of the guidance algorithm that was derived from the 2LON EOMs was more robust than the guidance formulation that was derived from the 3RSP EOMs when performing a direct entry. The above comparative studies indicate that guidance algorithms using simplified formulations perform better for mid- to low-L/D spacecraft flying a direct entry. Whereas, guidance algorithms that use higher fidelity formulations perform better for high L/D spacecraft flying a direct entry. Finally, if the mid- to low-L/D spacecraft is flying a skip/lofting trajectory, higher fidelity formulations outperform simplified formulations.

Guidance algorithm development was pioneered by Apollo Guidance engineers, including Moseley [38] and Graves and Harpold [39]. They had to develop a guidance algorithm that took up minimal computing resources while bringing the Apollo capsule, carrying United States astronauts, safely to Earth. Many in the entry guidance field still use the Apollo guidance algorithm given that it has been thoroughly flight tested and is simple to implement on-board.

There was an additional study, completed by engineers at NASA Johnson Space Center, that compared three guidance algorithms applied to the Aeroassist Flight Experiment (AFE) vehicle [40]. The Analytical Predictor Corrector (APC) [41], the Numeric Predictor Corrector (NPC), and the Energy Controller (EC) guided the AFE through an aerocapture trajectory. All three algorithms exhibited the same performance in the presence of dispersions, with no one algorithm being more robust than the other.

The European Space Agency has developed a guidance algorithm for a low L/D spacecraft called the Atmospheric Re-entry Demonstrator (ARD) and a mid L/D lifting body called the Intermediate Experimental Vehicle (IXV). The algorithm is a numeric predictor corrector that uses a family of predicted trajectories to determine the final guided trajectory that nulls the range error [28]. However, there is no comparative study to determine the relative robustness for this algorithm.

The aspect of including aerothermal parameters in guidance algorithms for mid- to low-L/D spacecraft is significantly different from high L/D spacecraft. Typically, the heat rate and/or heat load constraints are only considered when designing the trajectory for a given mission. This is because the control authority yields minimal changes to the heating profile. The heat rate and heat load are primarily sensitive to the entry state. Once the nominal trajectory is known, the heat rate is simply monitored during active guidance of dispersed trajectories. In the event that trajectories exceed the peak heat rate (or heat load) constraint, modifications to the vehicle shape and trajectory are proposed. For low- to mid-L/D spacecraft guidance heat load constraints are not considered.

4.3. Other planetary entry vehicles

Different guidance algorithms for Mars and Neptune are described in this section. The trajectory profiles for other planetary entry include aeroassist, aerocapture, and direct entry.

A joint effort between the Centre National d'Etudes Spatiales (CNES, France) and NASA Johnson Space Center was conducted to compare the Apollo derived Terminal Point Controller (TPC) [44], the Analytic Predictor Corrector (APC) [41,45,46], the Energy Controller (EC) [47], and the Numerical Predictor Corrector (NPC) [48,49] for the Mars Premier (MPrm, $L/D < 1$) vehicle performing an aerocapture maneuver [50]. It was found that the accuracy of the APC, in the presence of atmospheric dispersions, was better relative to the performance of the other algorithms. The more robust algorithm, with respect to the capture corridor and other dispersions, was the TPC.

Interestingly, the two guidance algorithms that have been improved upon, since the above comparison study, have been the TPC and APC. Specifically, guidance developers for Mars Smart Lander (MSLan) [51], Mars Science Laboratory (MSLab) [52], Neptune Ellipsled Vehicle (NEV) [53], Titan Blunt Body Aeroshell (TBB) [54], and HEMS [55] have used these algorithms. Guidance engineers for the Titan aerocapture mission completed a comparison of the APC and the TPC. It was found that the TPC had a much tighter distribution around the target orbit as compared to the distribution of cases in the APC. Both the TPC and the APC use the 2LON EOMs to develop a set of closed-form analytical solutions to describe the reference trajectory. This leads to very simple on-board implementation, however, these algorithms demand significant work to adapt for different missions and vehicles.

The TPC algorithm has been implemented on-board NASA MSLab mission and is a purely analytical algorithm. It is interesting to note that the simplicity of analytical algorithms is utilized in the majority of other planetary entry guidance algorithms. This does not mean that this type of guidance is more robust than numerical techniques, but that the predictability of guidance performance is high relative to the inherent uncertainty of other planetary atmospheres. There has been some development on numerical type guidance algorithms for other planetary entry. Mease et al. [56,57] have done significant work on adapting their X-33 guidance for a mid- to low-L/D vehicle performing a Mars direct entry.

There is another guidance method for aerocapture and/or direct entry of the Mars atmosphere, which modulates drag instead of the classical lift modulation approach. This algorithm uses a numeric predictor corrector to solve the 3RSP EOMS and the control variables include the change in the ballistic coefficient and the time of jettison [58,59]. Note that jettison is what changes the vehicles ballistic coefficient. Preliminary results of this algorithm show the potential to meet the same accuracy of current guidance algorithms while reducing system complexity. However, a comprehensive study, to compare robustness of this method with those discussed in the previous paragraph, has not been completed.

The aspect of including aerothermal parameters in guidance algorithms for other planetary entry vehicles of mid- to low-L/D is the same as for Earth entry. Typically, the heat rate and/or heat load are constraints when designing the trajectory for a given mission. The one exception is Jits et al. [60] who developed a numerical guidance algorithm for a Neptune direct entry which incorporated heat load as a trigger to activate targeting. This algorithm provides some insight into the possibility of managing heat loads during entry guidance.

5. Conclusion

This paper identified the fundamentals of planetary entry guidance and detailed the characteristics of the vast number of guidance algorithms that are in use today. The comparative studies for Earth entry guidance algorithms indicate that simplified formulations perform better for mid- to low-L/D spacecraft flying a direct entry. Whereas, guidance algorithms that use higher fidelity formulations perform better for high L/D spacecraft flying a direct entry. Finally, if the mid- to low-L/D spacecraft is flying a skip/lofting trajectory, higher fidelity formulations outperform simplified formulations. In addition, for other planetary entries, the simplicity of analytical algorithms is preferred given the relative uncertainties that exist. This does not mean that this type of guidance is more robust than numerical techniques, but that the predictability of guidance performance is high relative to the inherent uncertainty of other planetary atmospheres.

Finally, there are a few observations that can be made from this survey. First, the effort required to implement new missions for a

specific guidance algorithm appears to be a non-trivial task when the mission requirements or vehicle shape change. Second, most guidance developers do not apply optimal control formulations given known convergence issues. Third, the majority of guidance algorithms do not include management of entry heat rate or heat load in real-time.

Note that the authors of this publication welcome any feedback related to the technical content of this survey.

Acknowledgments

The authors would like to thank the NASA Ames Research Center Pathways Program and the Systems Design and Analysis Branch for funding this work in part.

References

[1] William KA. System requirements for the crew exploration vehicle element. Technical Report, CXP-10001; February 2006.
[2] Vinh NX, Busemann A, Culp R. Hypersonic and planetary entry flight mechanics. Ann Harbor: The University of Michigan Press; 1980.
[3] Vinh N. Optimal trajectories in atmospheric flight. Amsterdam, Oxford, New York: Elsevier Scientific Publishing Company; 1981.
[4] Leavitt JA, Saraf A, Chen D, Mease K. Performance of evolved acceleration guidance logic for entry (eagle). In: AIAA guidance, navigation, and control conference and exhibit, AIAA 2002-4456, Monterey, CA; 2002.
[5] Saraf A, Leavitt J, Chen D, Mease K. Design and evaluation of an acceleration guidance algorithm for entry. In: AIAA guidance, navigation, and control conference and exhibit, AIAA 2003-5737, Austin, TX; 2003.
[6] Leavitt JA, Mease K. Feasible trajectory generation for atmospheric entry guidance. J Guid Control Dyn 2007;30(2):473–81, http://dx.doi.org/10.2514/1.23034.
[7] Shen Z, Lu P. On-board generation of three-dimensional constrained entry trajectories. In: AIAA guidance, navigation, and control conference and exhibit. AIAA 2002-4455, Monterey, CA; 2002.
[8] Lu P, Hanson J, Bhargava S. An alternative entry guidance scheme for the x-33. In: AIAA guidance, navigation, and control conference, AIAA 1998-4255, Boston, MA; 1998.
[9] Lu P. Regulation about time-varying trajectories: precision entry guidance illustrated. J Guid Control Dyn 1999;22(6):784–90, http://dx.doi.org/10.2514/6.1999-4070.
[10] Lu P, Shen Z, Dukeman G, Hanson J. Entry guidance by trajectory regulation. In: AIAA guidance, navigation, and control conference and exhibit, AIAA 2000-3958, Denver, CO; 2000.
[11] Zimmerman C, Dukeman G, Hanson J. Automated method to compute orbital reentry trajectories with heating constraints. J Guid Control Dyn 2003;26(4):523–9, http://dx.doi.org/10.2514/2.5096.
[12] Dukeman GA. Profile-following entry guidance using linear quadratic regulator theory. In: AIAA guidance, navigation, and control conference and exhibit. AIAA 2002-4457, Monterey, CA; 2002.
[13] Hanson JM, Coughlin D, Dukeman G, Mulqueen J, McCarter J. Ascent, transition, entry, and abort guidance algorithm design for the x-33 vehicle. In: AIAA guidance, navigation, and control conference, AIAA 1998-4409, Boston, MA; 1998.
[14] Johnson EN, Calise AJ. Reusable launch vehicle adaptive guidance and control using neural networks. In: AIAA. AIAA 2001-4381; 2001.
[15] Schierman JD, Hull JR, Ward DG. Adaptive guidance with trajectory reshaping for reusable launch vehicles. In: AIAA guidance, navigation, and control conference and exhibit. AIAA 2002-4458, Monterey, CA; 2002.
[16] Hanson JM, Jones RE. Test results for entry guidance methods for space vehicles. J Guid Control Dyn 2004;27(6):960–6, http://dx.doi.org/10.2514/1.10886.
[17] Harpold JC, Graves CA. Shuttle entry guidance. J. Astronaut. Sci. 1979;27(3):239–68.
[18] Larson W, Pranke L, Connolly J, Gien R. Human spaceight: mission, analysis, & design. McGraw-Hill; 1999.
[19] Roenneke AJ, Markl A. Re-entry control to a drag-vs-energy profile.
[20] D'Souza S, Sarigul-Klijn N, Cerimele C. Development and simulation of an analytic skip earth re-entry guidance algorithm. In: AIAA space 2008 conference & exposition. AIAA 2008-7804, San Diego, CA; 2008.
[21] Schierman JD, Ward D, Hull J, Ghandi N, Oppenheimer M, Doman D. Integrated adaptive guidance and control for re-entry vehicles with flight-test results. J. Guid. Control Dyn. 2004;27(6):975–88, http://dx.doi.org/10.2514/1.10344.
[22] Fahroo F, Ross IM. Costate estimation by a Legendre pseudospectral method. J Guid Control Dyn 2001;24(2):270–7, http://dx.doi.org/10.2514/1.10344.
[23] Rea J. Launch vehicle trajectory optimization using a Legendre pseudospectral method. In: AIAA guidance, navigation, and control conference and exhibit. AIAA 2003-5640, Austin, TX; 2003.
[24] Rao AV, Clark KA. Performance optimization of a maneuvering re-entry vehicle using a Legendre pseudospectral method. In: AIAA atmospheric flight mechanics conference and exhibit. AIAA 2002-4885, Monterey, CA; 2002.
[25] Jorris TR. Common aero vehicle autonomous reentry trajectory optimization satisfying waypoint and no-fly zone constraints [Ph.D. thesis]. Air Force Institute of Technology, Ohio; September 2007.
[26] Mease KD, Chen D, Tandon S, Young D, Kim S. A three-dimensional predictive entry guidance approach. In: AIAA guidance, navigation, and control conference and exhibit, AIAA 2000-3959, Denver, CO; 2000.
[27] JD Schierman, D.Ward, Monaco J, Hull J. A recongurable guidance approach for reusable launch vehicles. In: AIAA, AIAA 2001-4429; 2001.
[28] Vernis P, Spreng F, Gelly G, Barrio AM. Accurate skip-entry guidance for low to medium l/d spacecrafts return mission requiring high range capabilities. in: AIAA guidance, navigation, and control conference and exhibit, AIAA 2011-6649, Portland, OR; 2011 39.
[29] Mooji E. Robust design methodology for a re-entry guidance system. In: AIAA guidance, navigation, and control conference and exhibit, AIAA 2001-4049, Montreal, Canada; 2001.
[30] Tigges M, Rea J, Johnson W, Crull T., Numerical skip-entry guidance. In: 30th annual AAS guidance and control conference, AAS-07-076, Breckinridge, CO; 2007.
[31] Putnam ZR. Improving lunar return entry range capability using enhanced skip trajectory guidance. J Spacecr Rockets 2008;45(2):309–15.
[32] Miller MA, et al. Managing energy and mode transitions in predguid entry guidance. In: AIAA guidance, navigation, and control conference and exhibit. AIAA 2008-7264, Honolulu, HI; 2008.
[33] Brunner CW, Lu P. Skip entry trajectory planning and guidance. J Guid Control Dyn 2008;31(5):1210–9.
[34] Putnam ZR, Neave M, Barton G. Predguid entry guidance for orion return from low earth orbit. In: IEEE aerospace conference, IEEEAC 1571, Big Sky, MT; 2010.
[35] Rea JR, Putnam Z. A comparison of two orion skip entry guidance algorithms. In: AIAA guidance, navigation, and control conference and exhibit, AIAA 2007-6424, Hilton Head, SC; 2007.
[36] Brunner C. W., Lu P. Comparison of numerical predictor-corrector and apollo skip entry guidance algorithms. In: AIAA guidance, navigation, and control conference, AIAA 2010-8307, Toronto, Canada; 2010.
[37] Lu P. Predictor–corrector entry guidance for low-lifting vehicles. J Guid Control Dyn 2004;31(4):1067–75.
[38] Moseley PE. The apollo entry guidance: a review of the mathematical development and its operational characteristics. Technical Report, TRW Note No. 69-FMT-791; 1969.
[39] Graves CA, Harpold JC. Apollo experience report—mission planning for apollo entry. Technical Report, NASA Technical Note, TN D-6725; March 1972.
[40] Gamble JD, Cerimele C, Moore T, Higgins J. Atmospheric guidance concepts for an aeroassist flight experiment. J. Astronaut. Sci. 1988;36(1):45–71, http://dx.doi.org/10.2514/3.21578 (53).
[41] Cerimele CJ, Gamble JD. A simplified guidance algorithm for lifting aeroassist orbital transfer vehicle. In: 23rd AIAA aerospace sciences meeting. AIAA 1985-0348, Reno, NV; 1985.
[42] Bairstow SH. Reentry guidance with extended range capability for low l/d spacecraft [Ph.D. thesis]. Massachusetts Institute of Technology, Massachusetts; February 2006.
[43] Cavallo A, Ferrara F. Atmospheric re-entry control for low lift/drag vehicle. J Guid Control Dyn 1996;19(1):47–53, http://dx.doi.org/10.2514/3.21578.
[44] Ro TU, Queen EM. Study of martian aerocapture terminal point guidance. In: AIAA atmospheric flight mechanics. AIAA 1998-4571, Boston, MA; 1998.
[45] Tigges M, Ling L. A predictive guidance algorithm for mars entry. In: AIAA aerospace sciences meeting. AIAA 1989-0632, Reno, NV; 1989.
[46] Masciarelli JP, Rousseau S, Frayesse H, Perot E. An analytical aerocapture guidance algorithm for the mars sample return orbiter. In: AIAA atmospheric flight mechanics conference, AIAA 2000-4116, Denver, CO; 2000.
[47] Rousseau S. An energy controller aerocapture guidance algorithm for the mars sample return orbiter. In: Advances in Astronautical Sciences, AAS 01-104; 2001.
[48] Powell RW. Numerical roll reversal predictor–corrector aerocapture and precision landing guidance algorithms for the mars surveyor program 2001 missions. In: AIAA atmospheric flight mechanics conference. AIAA 1998-4564, Boston, MA; 1998.
[49] Berges JC, Roussaeu S, Perot E. A numerical predictor corrector guidance algorithm for the mars sample return aerocapture. In: AAAF 14-66; 2001.
[50] S. Rousseau, E. Perot, C. Graves, J. Maciarelli, E. Queen, Aerocapture guidance algorithm comparison campaign, in: AIAA/AAS Astrodynamic Specialist Conference and Exhibit, AIAA 2002-4822, Monterey, CA, 2002.
[51] Mendeck GF, Ccarman GL. Guidance design for Mars smart landers using the energy terminal point controller. In: AIAA atmospheric flight mechanics conference and exhibit. AIAA 2002-4502, Monterey, CA; 2002.
[52] Mendeck GF, Craig LE. Entry guidance for the 2011 Mars science laboratory mission. In: AIAA atmospheric flight mechanics conference and exhibit. AIAA 2011-6639, Portland, OR; 2011.
[53] Masciarelli JP, Westhelle C, Graves C. Aerocapture guidance performance for the Neptune orbitor. In: AIAA atmospheric flight mechanics conference and exhibit, AIAA 2004-4954, Providence, RI; 2004.
[54] Masciarelli JP, Queen EM. Guidance algorithms for aerocapture at titan. In: AIAA/ASME/SAE/ASEE joint propulsion conference and exhibit, AIAA 2003-4804, Huntsville, AL; 2003.

[55] Zumwalt CH, Sostaric R, Westhelle C. Aerocapture guidance and performance at mars for high mass systems. In: AIAA/AAS astrodynamics specialist conference, AIAA 2010-7971, Toronto, Canada; 2010.
[56] Tu K. Drag-based predictive tracking guidance for mars precision landing. J. Guid. Control Dyn. 2000;23(4):620–8.
[57] Benito J, Mease K. Mars entry guidance with improved altitude control. In: AIAA/AAS astrodynamics specialist conference and exhibit, AIAA 2006-6674, Keystone, CO; 2006.
[58] Putnam ZR, Clark I, Braun R. Drag modulation ight control for aerocapture. In: IEEE aerospace conference; 2012 43.
[59] Putnam ZR, Braun RD. Precision landing at mars using discreteevent drag modulation, J. Spacecr. Rockets.
[60] Jits R, Wright M, Chen Y-K. Closed-loop trajectory simulation for thermal protection system design for neptune aerocapture. J. Spacecr. Rocket 2005;42 (6):1025–34.
[61] Bates RR, Miller DD, White JE. Fundamentals of astrodynamics. Dover Publications, Inc.; 1971.
[62] Streipe SA, Queen E, Powell R, Braun R, Cheatwood F, Aguirre J, et al., An atmospheric guidance algorithm testbed for the mars surveyor program 2001 orbiter and lander. In: AIAA atmospheric flight mechanics conference, AIAA 1998-4569, Boston, MA; 1998.
[63] Steinfeldt BA, Tsiotras P. A state-dependent Riccati equation approach to atmospheric entry guidance. In: AIAA guidance, navigation, and control conference. AIAA 2010-8310. Toronto, Canada; 2010.
[64] Kluever CA. Entry guidance performance for mars precision landing. J Guid Control Dyn 2008;31(6):1537–44.